Supporting Information

Impact of Fluorination Degree of Ether-Based Electrolyte Solvent on Li-metal Battery Performance

Yangju Lin,[1‡] Zhiao Yu,[1,2‡] Weilai Yu,[1] Sheng-Lun Liao,[1] Elizabeth Zhang,[1,3] Xuelin Guo,[1] Zhuojun Huang,[1,3] Yuelang Chen,[1,2] Jian Qin,*[1] Yi Cui*[3,4,5] and Zhenan Bao*[1]

[1]Department of Chemical Engineering, [2]Department of Chemistry, and [3]Department of Materials Science and Engineering, [4]Department of Energy Science and Engineering, Stanford University, Stanford, California 94305, United States.

[5]Stanford Institute for Materials and Energy Sciences, SLAC National Accelerator Laboratory, Menlo Park, California 94025, United States.

Table of Contents

I. General chemicals and materials

Chemicals. 2-Fluoroethanol was purchased from Matrix Scientific, and 2,2-difluoroethanol was purchased from SynQuest Labs, Inc. Lithium bis(fluorosulfonyl)imide (LiFSI) were obtained from Arkema. 2-Ethoxyethanol, tosyl chloride (TsCl), triethyl amine (Et_3N), triethylene glycol, ethylene carbonate, and tetraethylene glycol dimethyl ether (TEGDME) were purchased from Sigma-Aldrich. Sodium hydride (NaH, 60wt% dispersion in Paraffin liquid) was purchased from TCI Chemicals. Tetrabutylammounium fluoride (TBAF) solution (1 M in THF) was obtained from Acros Organics through Fisher Scientific. Other common solvents, including deuterium oxide (D_2O), chloroform-*d* ($CDCl_3$), dichloromethane (DCM), and dry tetrahydrofuran (THF) were used without further purification.

Materials. Lithium foil (50 μm) was obtained from Uniglobe Kisco Inc. Celgard 2325 separator (25 μm thick, polypropylene/polyethylene/polypropylene trilayer) was purchased from Celgard. Cu current collector (25 μm thick) was purchased from Alfa Aesar. Lithium chips (600 μm), 2032-type battery casings, stainless steel spacers, springs, Pt-clad and Al-clad coin cell cases were purchased from MTI. NMC811 cathode sheets (ca. 4.8 mAh/cm^2, 20.47 mg/cm^2 active materials) were purchased from Targray. Commercial dry Cu||LFP pouch cells were purchased from Li-Fun Technology.

II. Characterization

NMR spectra. ^{1}H, ^{19}F and ^{13}C NMR spectra were obtained on a Varian or Bruker 400 MHz NMR spectrometer using $CDCl_3$ as solvent at ambient temperature, and the chemical shift was referenced to the residual $CHCl_3$ (7.26 ppm for ^{1}H and 77.16 ppm for ^{13}C). ^{7}Li NMR spectra of electrolytes were recorded using 1 M LiCl solution in D_2O as an external reference (0.00 ppm), through a setup of a capillary tube in the NMR tube.

Raman spectra. The Raman spectra of electrolytes solution were obtained on a Horiba XploRA+ confocal Raman in transmission mode with a 532 nm excitation laser. The electrolyte solutions were prepared in the Ar-filled glovebox and sealed in narrow (0.1 cm width) quartz cuvettes. Due to the error in instrument calibration, the obtained spectra were calibrated using a DEE electrolyte, which was referenced to a reported value by a blueshift of 10 cm^{-1}.

Coin cell fabrication. All electrochemical measurements were performed using the 2032-type coin cells under ambient conditions, and coin cell fabrication was performed in an Ar-filled glovebox. In a typical procedure, e.g., Li||Cu half-cell, a spring was placed in a negative coin cell case, followed by a stainless steel and a thick Li foil (600 μm) with diameter of 7/16 inch. Then, 20 μL of electrolyte was added to the surface of Li foil and one piece of Celgard 2325 separator was placed on top of Li foil, followed by addition of another 20 μL of electrolyte. Finally, a Cu foil and the stainless-steel positive case were placed sequentially. The coin cell was then subjected to crimper press.

For fabrication of Li||Al and Li||Pt cells, the Al-clad or Pt-clad case was used instead. Notably, an additional Al foil was placed inside the Al cathode case to avoid the potential undesired impact related to the defects in the Al cladding.

In Li||NMC coin cells, a 50 μm thin Li foil (ca. 10.3 mAh/cm^2) and a high-loading NMC811 cathode (ca. 4.8 mAh/cm^2) were used, which give a N/P ratio of ~2.1, and an additional Al foil was placed between the NMC811 cathode and Al case as well.

Pouch cell preparation. The commercial dry Cu||LFP pouch cell was use for the pouch cell fabrication. Specifically, the pouch cell was open in the glovebox, and 500 μL liquid electrolyte (E/C ~2.4 g/Ah) was injected to the pouch and equilibrate for overnight. The pouch cell was then sealed and subjected to cycling test (C/2, 2D) using an Arbin cycler.

Electrochemical measurements. Electrochemical Impedance Spectroscopy (EIS) and linear sweep voltammetry (LSV) were measured on a Biologic VSP300 Potentiostat station. Li||Cu and Li|NMC cells were tested on Land or Arbin battery testing stations.

The EIS was run at the frequency range of 1 MHz ~ 100 mHz using stainless steel (SS) symmetric cells (SS||SS). The LSV was recorded at a scanning rate of 1 mV/s using Li||Al and Li||Pt cells, and the leakage current density was calculated based on an electrode area of 2.11 cm^2.

Full-cell cycling were performed between 2.8 and 4.4 V, and two formation cycles were performed at a charge and discharge current density of 0.4 mA/cm^2. For long-term cycling, cells were charged at 0.8 mA/cm^2 (~C/5) and held at 4.4 V until current reaches < 0.2 mA/cm^2 and discharged at 1.3 mA/cm^2 (~D/3).

CE measurements and long-term Li cycling were performed using Li||Cu half cells. CEs were measured by a modified Aurbach mothod, in which the Cu surface was first conditioned (or "cleaned") by plating 5 mAh/cm^2 of Li and stripping to 1 V at current density of 0.5 mA/cm^2. Then, a Li reservoir of 5 mAh/cm^2 was plated onto Cu, followed by 10 cycles of Li plating/striping at current density of 1 mAh/cm^2 and 0.5 mA/cm^2, respectively. In the final step, all Li on Cu was stripped to 1 V at current density of 0.5 mA/cm^2. For the long-term cycling, a Cu-conditioning procedure was performed by holding at 0.01 V for 5 h and then cycled between 0 and 1 V at 0.2 mAh/cm^2 for 10 cycles. Next, 1 mAh/cm^2 of Li was plated onto Cu surface and then stripped to 1 V at current density of 0.5 mAh/cm^2 (C/2, D/2).

SEM and XPS characterization. The morphology of Li deposition on Cu surface was studied by depositing 0.1 mAh/cm^2 of Li at 0.5 mAh/cm^2 current density using Li||Cu cells. Like long-term Li cycling in Li||Cu cells, the Cu substrates were first conditioned before Li deposition. After Li deposition, the cells were disassembled, and the Cu electrodes were rinsed with DME solvent and transferred into an airtight vessel to avoid air exposure. Same procedures were performed for samples subjected to XPS analysis of SEI composition, with the difference that 1 mAh/cm^2 was deposited in the 1st or 10th cycle. The XPS data were recorded on a PHI VersaProbe III with Al Kα radiation. The samples were sputtered with an Ar^+ ion gun at low power (1 kV, 0.7 μA, 2 mm×2 mm) to obtain the depth profiles.

XRD analysis. Li||NMC811 full cells using various electrolytes were subjected to 2 activation cycles (C/10, D/10) and then 10 charging/discharging cycles (C/5, D/3) in the voltage range of 2.8–4.4V. The fully discharged cells were then disassembled, and the NMC cathodes were placed on a substrate and sealed with a Kapton tape. The samples were analyzed using a Rigaku Miniflex instrument with Cu K-α X-ray source. The range of scanning angle was set to 10–80 °.

III. Computational study

MD simulations were carried out using Gromacs 2021.3[1] with the general amber force field (GAFF).[2] Topology files were generated using ACPYPE,[3] and the atomic partial charges were calculated by the restrained electrostatic potential (RESP) fitting approach in antechamber 22.063, where the quantum mechanical molecular electrostatic potential was computed by Gaussian16 at the B3LYP/6-311** level. Due to a non-polarizable force field, partial charges for charged ions were scaled by factors ranging from 0.8 to account for electronic screening.

The simulation box, subjected to three-dimensional periodic boundary conditions, was composed of 400 LiFSI and an appropriate number of solvent molecules to match the prescribed concentration. The simulation began with randomly distributed ions and solvent molecules. Electrolytes and ions were equilibrated for 20 ns in an NPT ensemble using the Parrinello-Rahman barostat at 1 bar, with a time step of 1 fs, followed by 20 ns production run. MD trajectory data were stored every 5 ps. A Nosé-Hoover thermostat was applied throughout with a reference temperature of 300 K. The presented results were generated from the production run. The particle mesh Ewald method was used to calculate electrostatic interactions, with a real-space cut-off of 1 nm and a Fourier spacing of 0.16 nm. The Verlet cut-off scheme was used to generate pair lists. A cut-off of 1 nm was used for non-bonded Lennard-Jones interactions, and bonds with hydrogen atoms were constrained.

The visualizations were generated with VMD.[4] Solvation statistics were calculated using the MDAnalysis Python package.[5, 6]

IV. Synthesis of fluorinated ether molecules

Scheme S1 Synthetic scheme of fluorinated ether molecules

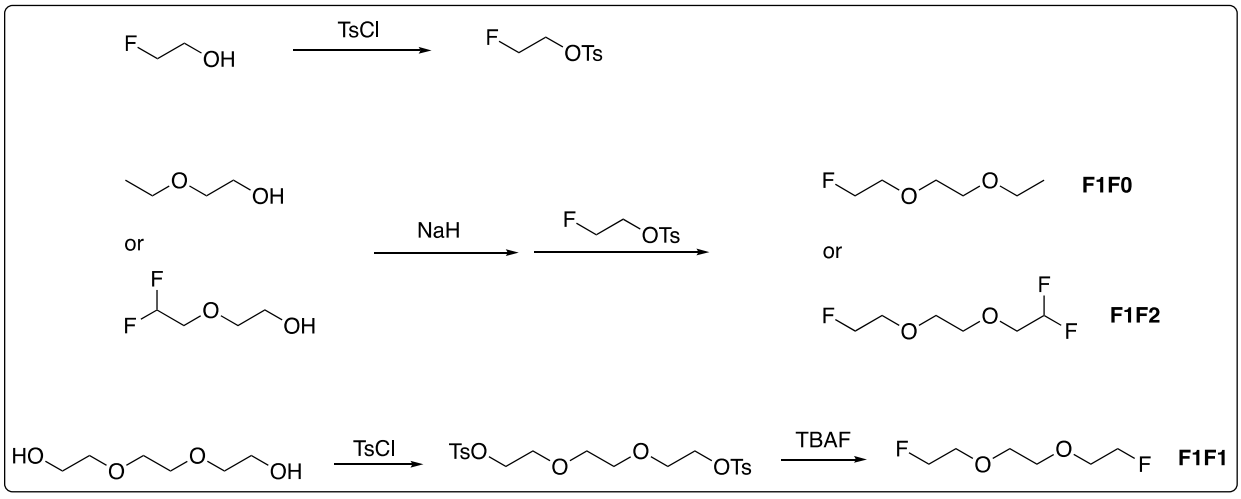

1. Synthesis of 2-fluoroehtyl tosylate

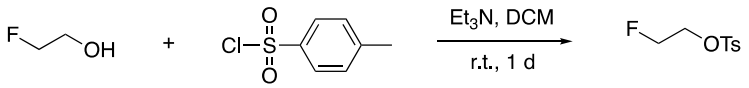

To a solution of 2-fluoroethanol (25 g, 0.391 mol) in 200 mL DCM, added Et_3N (65.2 mL, 0.469 mol). A solution of tosyl chloride (81.64 g, 0.430 mol) in 200 mL DCM was then slowly added into above mixture over 20 min. The reaction was then stirred at room temperature for one day, after which the DCM phase was washed with 2×300 mL DI water, 300 mL aqueous $NaHCO_3$ solution (1 M), 300 mL DI water and then 300 mL brine. DCM phase was then collected and dried with anhydrous $MgSO_4$. After filtration, DCM was

removed by rotavap, and the product was obtained as a pale orange liquid (85.32 g, ~100% crude yield), which was used without further purification. ^{1}H NMR (400 MHz, $CDCl_3$): δ = 7.78 (d, J = 8.4 Hz, 1H), 7.38 – 7.30 (m, 2H), 4.64 – 4.57 (m, 1H), 4.53 – 4.46 (m, 1H), 4.30 – 4.24 (m, 1H), 4.23 – 4.17 (m, 1H), 2.43 (d, J = 0.7 Hz, 3H).

2. Synthesis of **F1F0** solvent molecule

2-Ethoxyethanol (15.8 mL, 0.164 mol) was dissolved with 150 mL dry THF, and the solution was cooled with an ice bath. NaH (7.194 g, 60 wt%, 0.180 mol) was added in portions to the solution. The mixture was further stirred for 2 h, after which 2-fluoroehtyl tosylate (37.26 g, 0.172 mol) was added. The resulting mixture was further stirred for 2 h and then refluxed overnight. After cooled to room temperature, insoluble solid was filtered and rinsed with THF. Combined THF solution was condensed, and the final product was obtained as a colorless liquid after five times of vacuum distillation (~0.2 torr, 22~25 °C, 12.0 g, 53.8% yield). ^{1}H NMR (400 MHz, $CDCl_3$): δ = 4.57 (m, 2H), 4.45 (m, 2H), 3.74 (m, 2H), 3.69 – 3.62 (m, 6H). ^{19}F NMR (400 MHz, $CDCl_3$): δ = -222.98 (tt, J = 47.7, 29.5 Hz). ^{13}C NMR (100 MHz, $CDCl_3$): δ = 84.16, 82.48, 71.04, 70.66, 70.46, 69.98, 66.84, 15.27.

3. Synthesis of **F1F2** solvent molecule

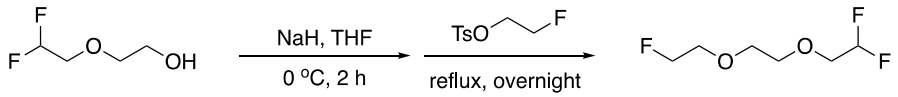

The procedure for synthesizing **F1F2** is similar to **F1F0**. 2-(2,2-difluoroethoxy)ethanol[7] (25.2 g, 0.20 mol), NaH (8.8 g, 60 wt%, 0.22 mol) and 2-fluoroehtyl tosylate (47.74 g, 0.22 mol) were used, and the final product was obtained as a colorless liquid after five times of distillation (~0.2 torr, 55 °C 16.2 g, 47.1% yield). ^{1}H NMR (400 MHz, $CDCl_3$): δ = 6.08 – 5.66 (m, 1H), 4.68 – 4.59 (m, 1H), 4.55 – 4.47 (m, 1H), 3.86 – 3.63 (m, 9H). ^{19}F NMR (400 MHz, $CDCl_3$): δ = -125.18 (dt, J = 55.5, 14.0 Hz), -223.07 (tt, J = 47.7, 29.7 Hz). ^{13}C NMR (100 MHz, $CDCl_3$): δ = 83.93, 82.25, 70.75, 70.50, 70.30.

4. Synthesis of **F1F1** solvent molecule

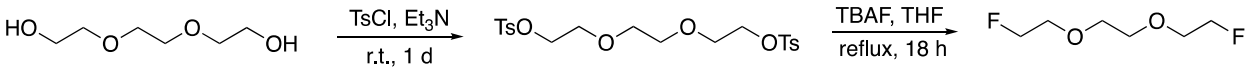

Triethylene glycol (30.0 g, 0.2 mol) and Et_3N (64 mL, 0.46 g) were dissolved with 300 mL DCM. The solution was cooled with an ice bath, and tosyl chloride (76.0 g, 0.44 mol) in 300 mL DCM was then added slowly into the solution over 20 min. The reaction was slowly warmed to room temperature and stirred for one day, and solid ammonium salt generated after the reaction. The mixture was then washed with 2×400 mL DI water, 400 mL aqueous $NaHCO_3$ solution (1 M), 400 mL DI water and then 400 mL brine. DCM phase was collected and dried over $MgSO_4$. After filtration and condensation, the product was obtained as an off-white solid. 400 mL TBAF solution in THF (1M) was then added, and the mixture was warm up to reach complete dissolution. The reaction was then refluxed for 18 h and then cooled to room temperature. THF was then removed to give a viscous liquid, and product was first isolated by vacuum distillation (76~78 °C, ~7.5 torr). The temperature was finally raised to 130 °C to ensure the isolation of product from the viscous bulk. The obtained liquid was further subjected to four times of vacuum distillation to give final product (~0.2 torr, 27~30 °C, 22.3 g, 72.4%). ^{1}H NMR (400 MHz, $CDCl_3$): δ = 4.57 (m, 2H), 4.45 (m, 2H), 3.74 (m, 2H), 3.69 – 3.62 (m, 6H). ^{19}F NMR (400 MHz, $CDCl_3$): δ = -223.13 (tt, J = 50.8, 29.6 Hz). ^{13}C NMR (100 MHz, $CDCl_3$): δ = 83.93, 82.25, 70.75, 70.50, 70.30.

V. Characterization of electrolytes

Electrolytes were prepared by dissolving 1.2 mmol of LiFSI salt in 1 mL solvent molecule. The electrolytes were shaken and set at room temperature overnight before use. The electrolytes were subjected to analysis of ionic conductivity and solvation by NMR.

Table S1 Parameters of prepared electrolytes

	DEE	**F1F0**	**F1F1**	**F1F2**
Solvent molecular weight	118.17	135.17	154.16	172.15
Solvent density (g/mL)	0.842	0.982	1.116	1.193
Solvent/LiFSI ratio	5.94	6.01	6.03	5.78

Table S2 Viscosity of prepared electrolytes (unit: mPa·s)

Trial	**F1F0**	**F1F1**	**F1F2**
1	3.744	7.139	7.667
2	3.749	7.135	7.657
3	3.756	7.127	7.658
4	3.746	7.132	7.676
5	3.758	7.136	7.661
Avg.	3.751	7.134	7.664
SD	0.006	0.004	0.008

1. Ionic conductivity

The coin-cell setup (described in **II. characterization**) was applied for ionic conductivities measurements. Each electrolyte was measured three times and results were shown in Table S2.

Table S3 Summary of ionic conductivities of prepared electrolytes (unit: S/cm)

	DEE	**F1F0**	**F1F1**	**F1F2**
Trial 1	3.58E-04	5.12E-04	3.23E-04	2.92E-04
Trial 2	3.24E-04	5.91E-04	3.33E-04	3.11E-04
Trial 3	3.38E-04	5.64E-04	3.32E-04	3.30E-04
Avg.	3.40E-04	5.56E-04	3.29E-04	3.11E-04
SD.	1.73E-05	3.99E-05	5.61E-06	1.89E-05

2. NMR study of solvation

The ^{7}Li and ^{19}F NMR of electrolytes were recorded and compared with that of pure solvent molecules. The ^{7}Li NMR is provided in the manuscript and ^{19}F NMR is shown in Figure S1.

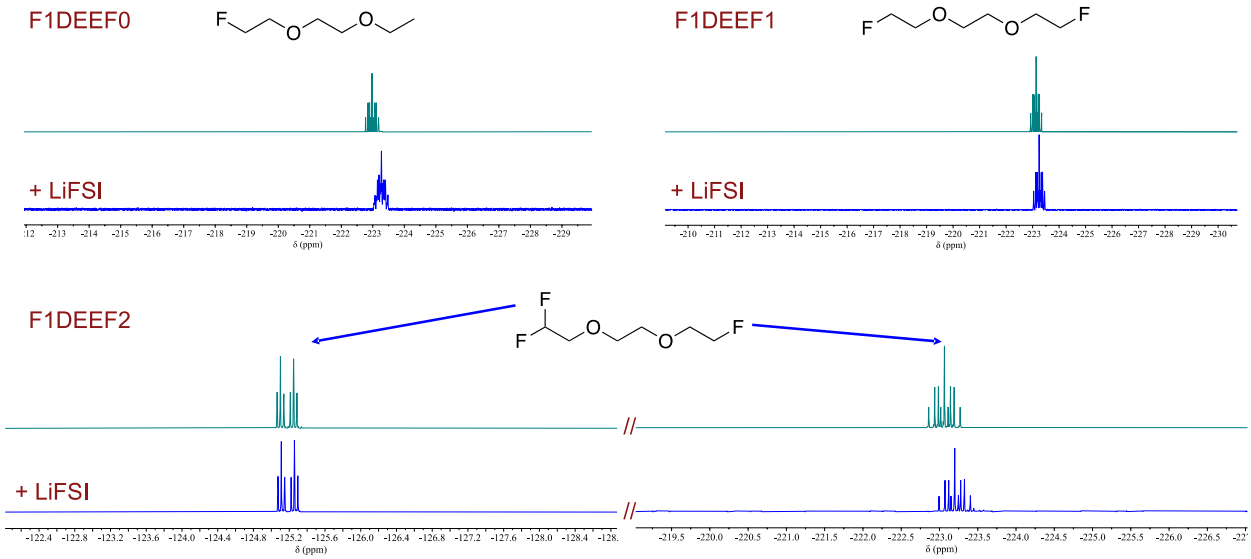

Figure S1 ^{19}F NMR spectra of solvents and electrolytes. Only the peaks associated with solvent fluorine are shown. It seems that the signals of monofluoride substituent slightly shift to up field region, indicating the interaction with salt.

3. Raman analysis of solvation

The full spectra of investigated electrolytes are provided in Figure S2.

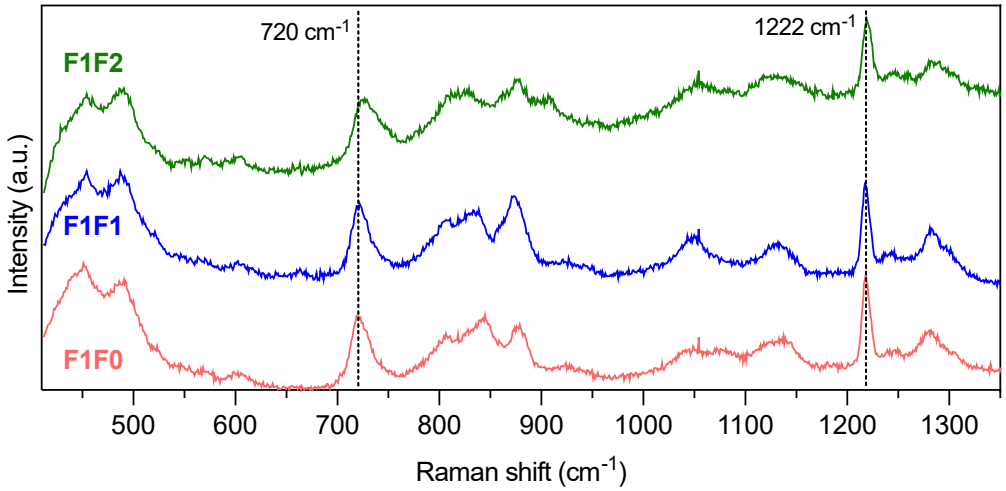

Figure S2 Stack of Raman spectra of electrolytes with 1.2 M LiFSI salt.

4. Oxidative stability measurement by LSV using Li||Pt cells

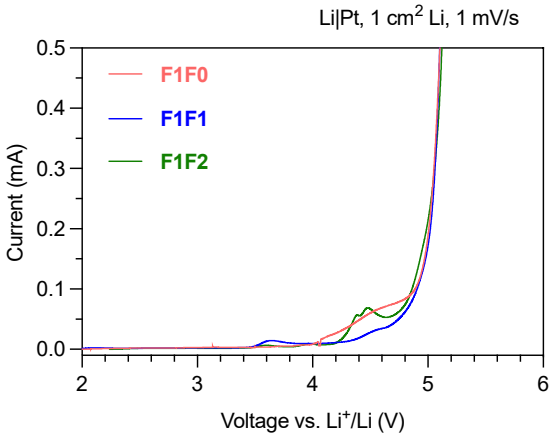

Figure S3 Linear sweep voltammetry of electrolytes containing 1.2M LiFSI using Li||Pt cell to avoid the corrosion uncertainty from using Al counter electrode. Scanning rate 1mV/s.

VI. Full cell performance

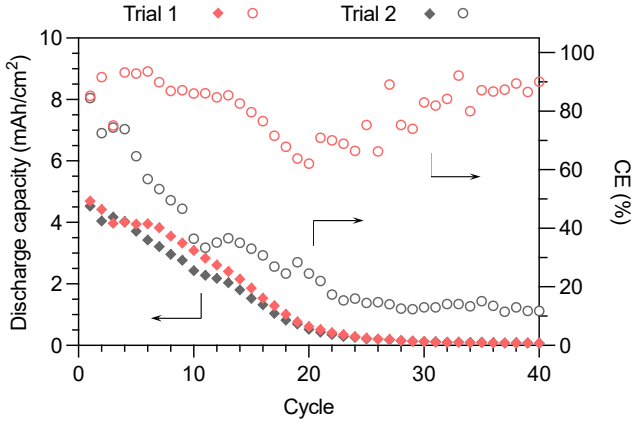

Figure S4 Areal discharge capacity of Li||NMC811 full cells over cycling numbers using **F1F0** electrolyte solvent. 4.8 mAh/cm^2, C/5 charging and D/3 discharging.

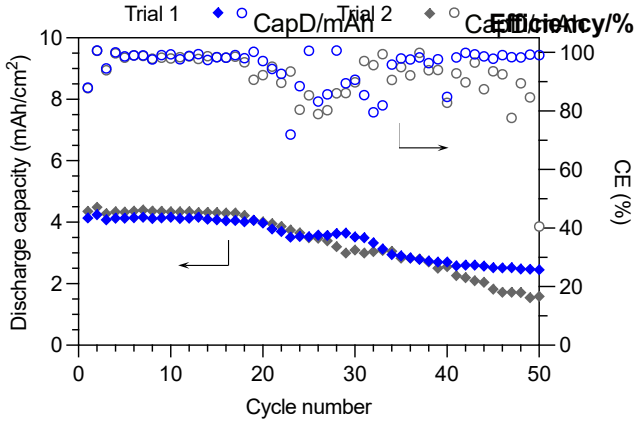

Figure S5 Areal discharge capacity of Li||NMC811 full cells over cycling numbers using **F1F1** electrolyte solvent. 4.8 mAh/cm^2, C/5 charging and D/3 discharging.

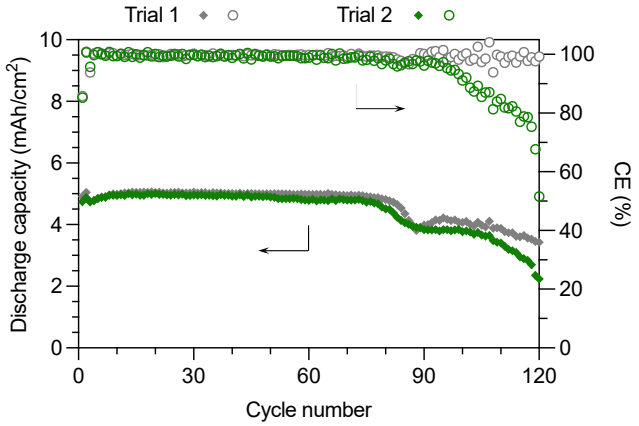

Figure S6 Areal discharge capacity of Li||NMC811 full cells over cycling numbers using **F1F2** electrolyte solvent. 4.8 mAh/cm^2, C/5 charging and D/3 discharging.

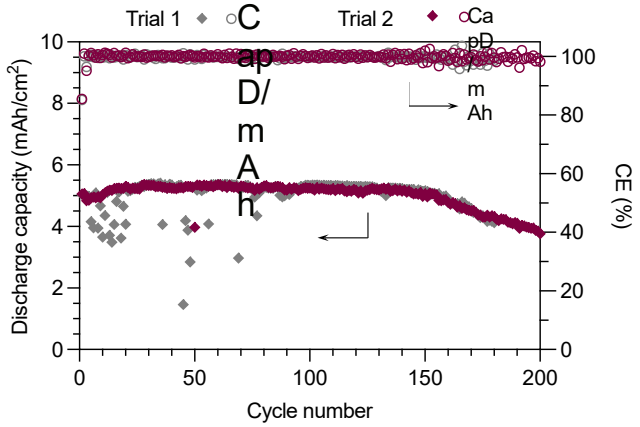

Figure S7 Areal discharge capacity of Li||NMC811 full cells over cycling numbers using **F5DEE** electrolyte solvent. ~5 mAh/cm^2, C/5 charging and D/3 discharging. Note: data was adapted from previous results.[7]

VII. XRD analysis of NMC cathode after cycling

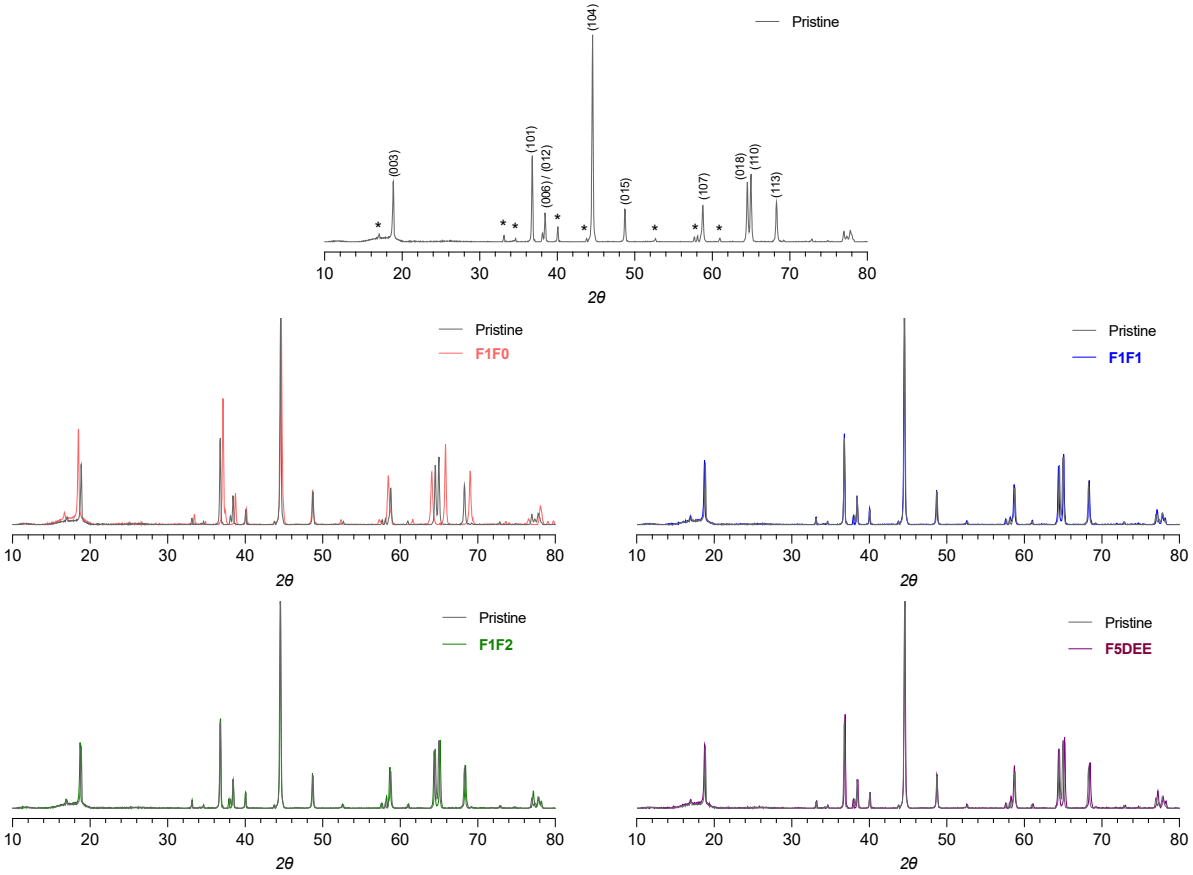

Figure S8 XRD analysis of pristine cathode and cathode materials after 10 cycles using various electrolytes in the Li||NMC811 full cells. The top spectrum indicates the XRD of pristine NMC811 electrode as we used, and the impure peaks labeled with "*" could be due to the degradation/surface degradation after storage in the glovebox. Only F1F0 showed significant peak shift after 10 cycles, and other electrolytes indicated high structural integrity with minor noticeable shift at (003), (018), (110) and (113) peaks.

VIII. Cycling of Li

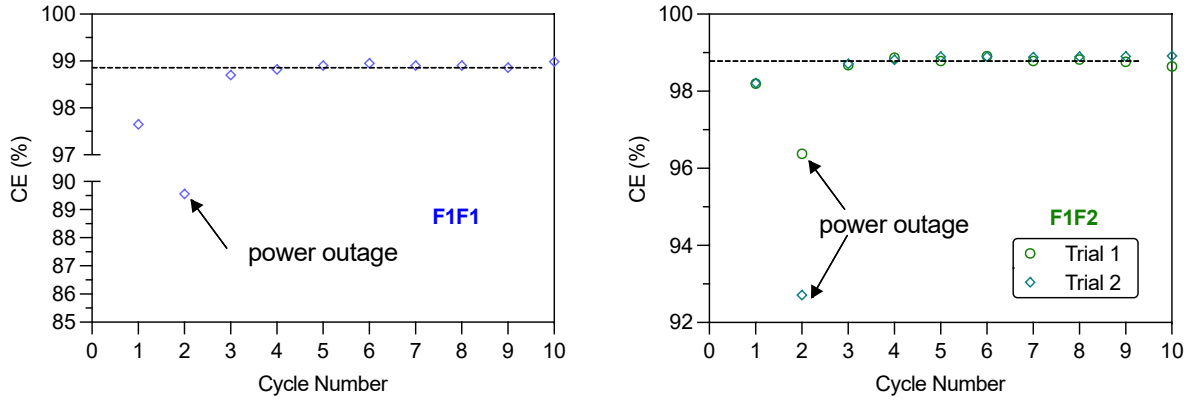

Figure S9 Initial 10 cycles of Li plating/stripping using **F1F1** (left) and **F1F2** (right) electrolytes in Li||Cu cells.

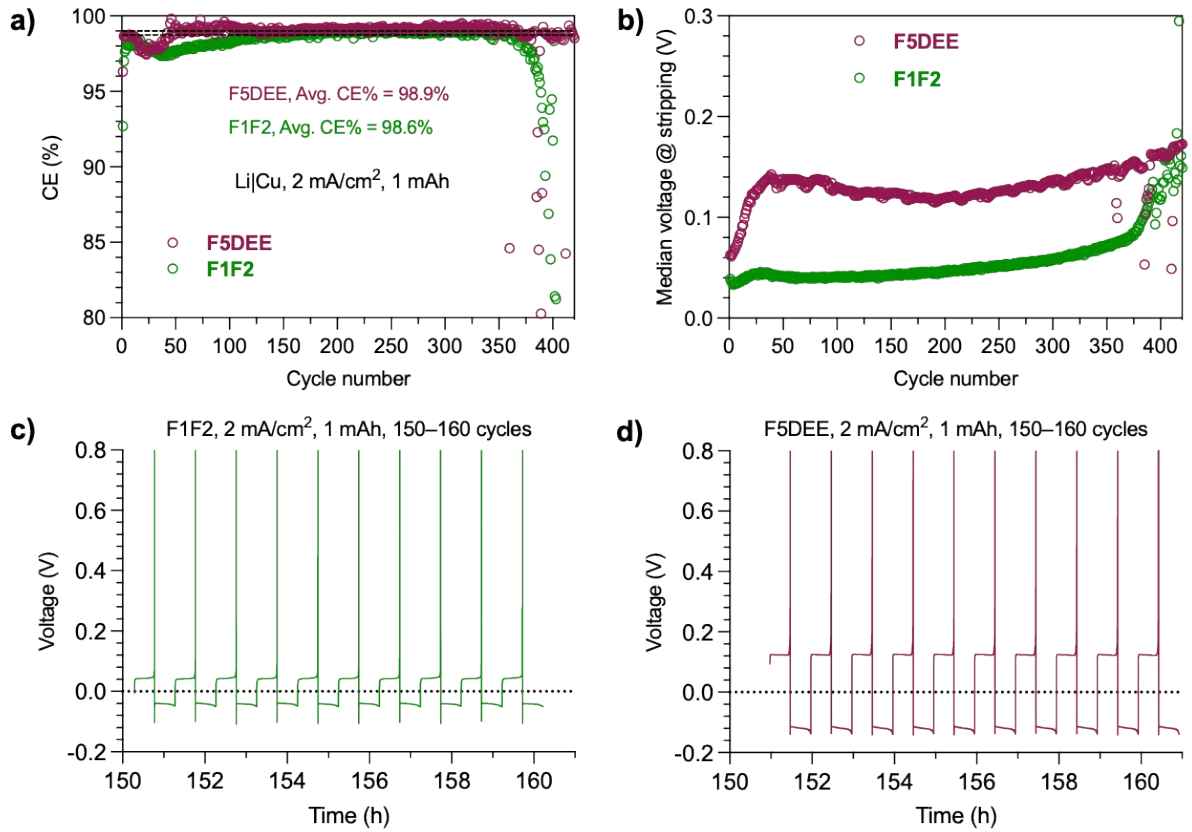

Figure S10 Li plating/stripping using **F1F2** and **F5DEE** electrolyte at 2 mA/cm^2 current density. (a) **F1F2** and **F5DEE** show comparable stability of Li cycling, while **F5DEE** show slightly higher average CE than **F1F2** (98.9% vs. 98.6%). In both cases, CE starts to drop at ~370 cycles, whereas **F5DEE** seems to be more like scattering instead of drop in the later cycles. b) Comparison of median overpotential at stripping over cycle numbers. It is evident that **F1F2** shows a much lower overpotential than F5DEE (~40 mV vs. ~130 mV), and it would be potential beneficial for charging under high current density. Voltage curves of **F1F2** c) and **F5DEE** d) electrolytes at 150–160 cycles of Li cycling.

IX. Characterization of Li deposition

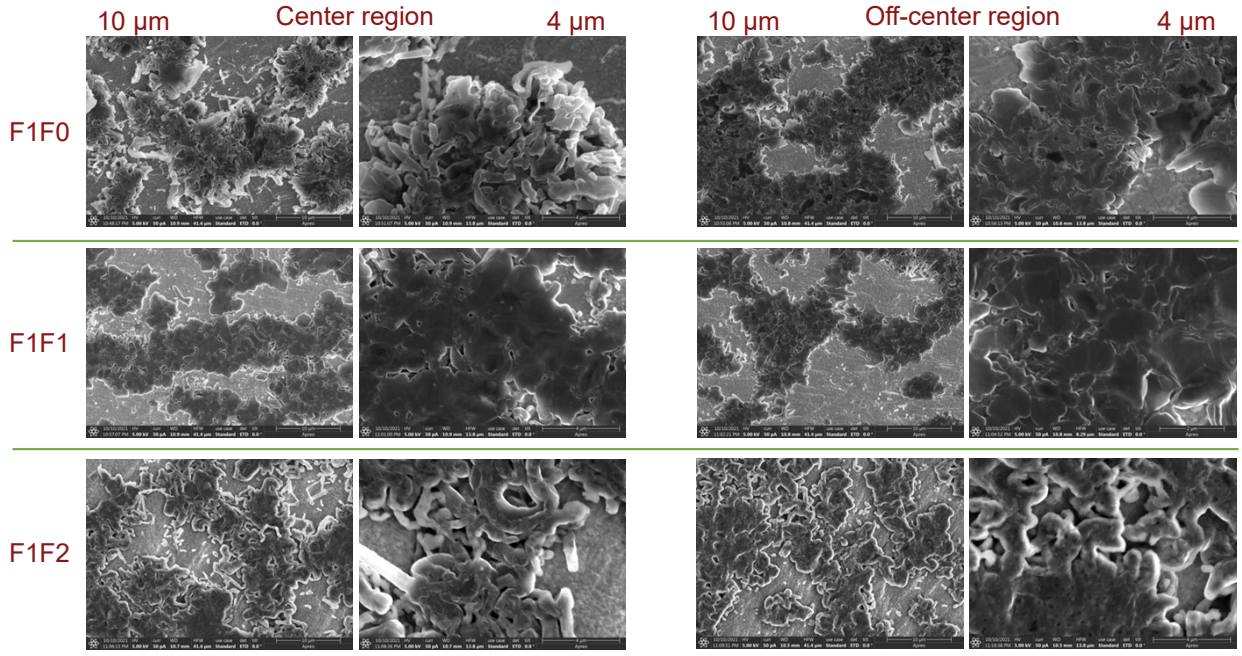

Figure S11 SEM imaging of Li deposition using **F1F0** (top), **F1F1** (middle), and **F1F2** (bottom) electrolytes. The depositions of Li were performed using Li||Cu cells. The Cu was activated by galvanostatic cycling at 0.2 mA between 0–1 V for 10 cycles, and 0.1 mAh of lithium was then plated on Cu at 0.5 mA/cm^2 current density. Center (left column) and off-center (right column) regions on the Cu electrode were examined.

X. SEI analysis

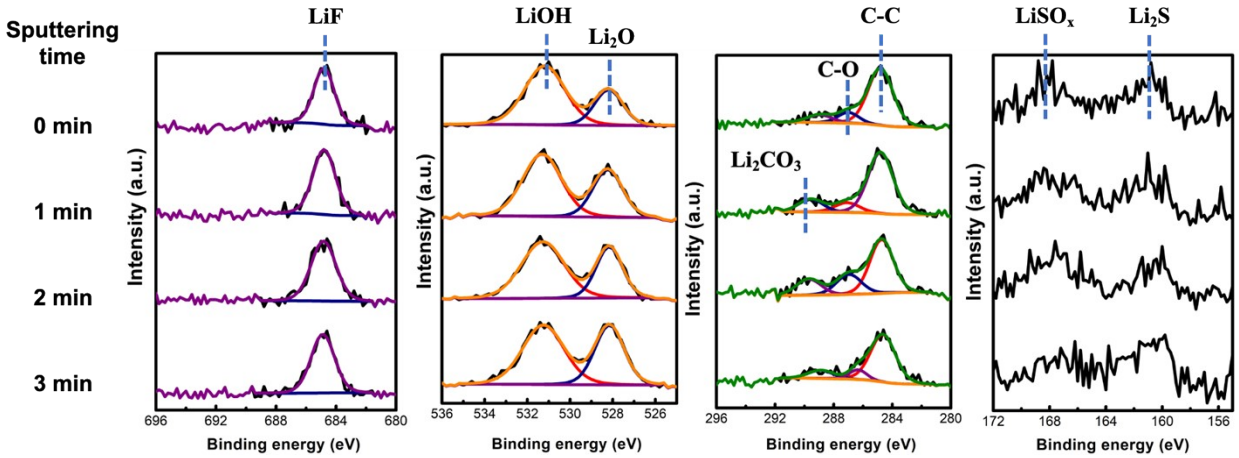

Figure S12 XPS spectra of SEI composition on Li surface using **F1F0** electrolyte. The Li||Cu cell was cycled between 0 and 1 V at 0.2 mAh/cm^2 for 10 cycles and then deposited with 1 mAh/cm^2 Li on Cu at 0.5 mA/cm^2. The Li surface was rinsed with DME solvent and then subjected to XPS analysis. The surface was further sputtered for various times to inspect the SEI composition.

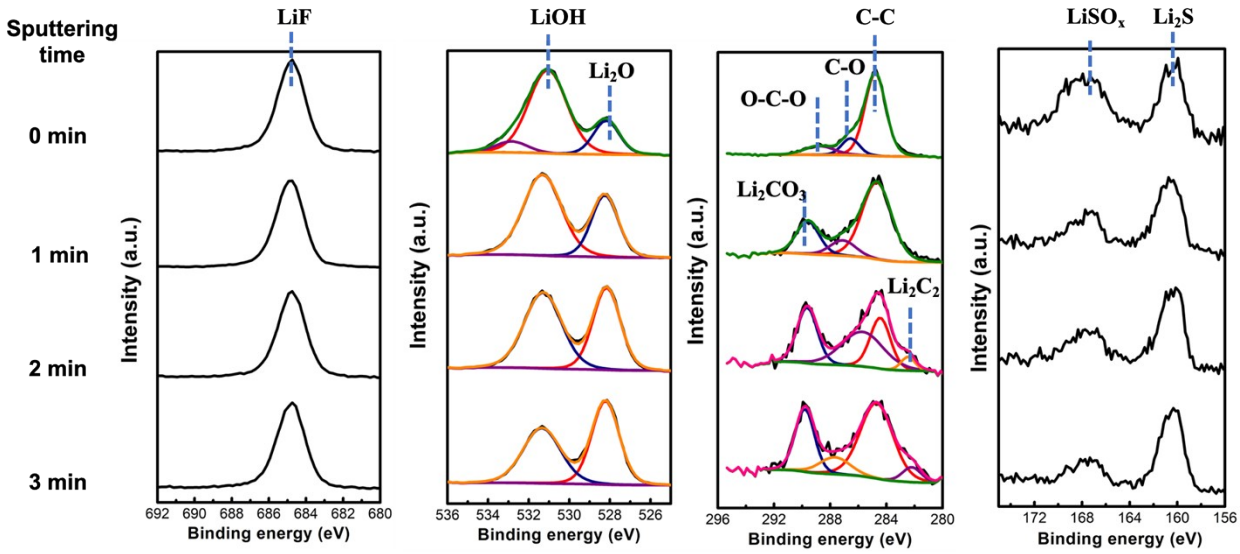

Figure S13 XPS spectra of SEI composition on Li surface using **F1F1** electrolyte. The Li||Cu cell was cycled between 0 and 1 V at 0.2 mAh/cm^2 for 10 cycles and then deposited with 1 mAh/cm^2 Li on Cu at 0.5 mA/cm^2. The Li surface was rinsed with DME solvent and then subjected to XPS analysis. The surface was further sputtered for various times to inspect the SEI composition.

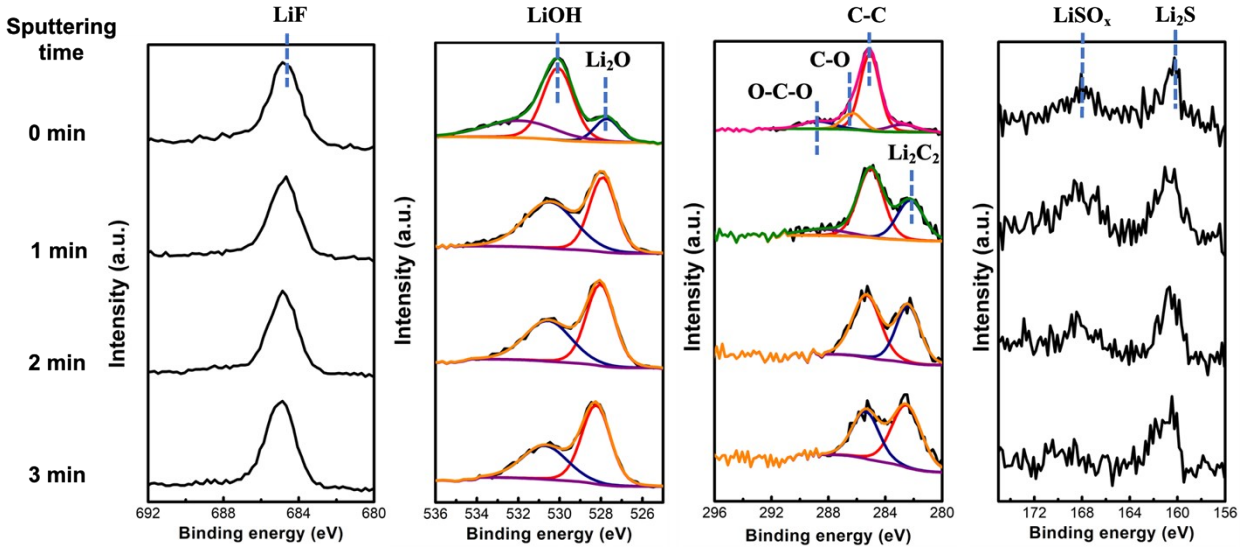

Figure S14 XPS spectra of SEI composition on Li surface using **F1F2** electrolyte. The Li||Cu cell was cycled between 0 and 1 V at 0.2 mAh/cm^2 for 10 cycles and then deposited with 1 mAh/cm^2 Li on Cu at 0.5 mA/cm^2. The Li surface was rinsed with DME solvent and then subjected to XPS analysis. The surface was further sputtered for various times to inspect the SEI composition.

XI. NMR spectra

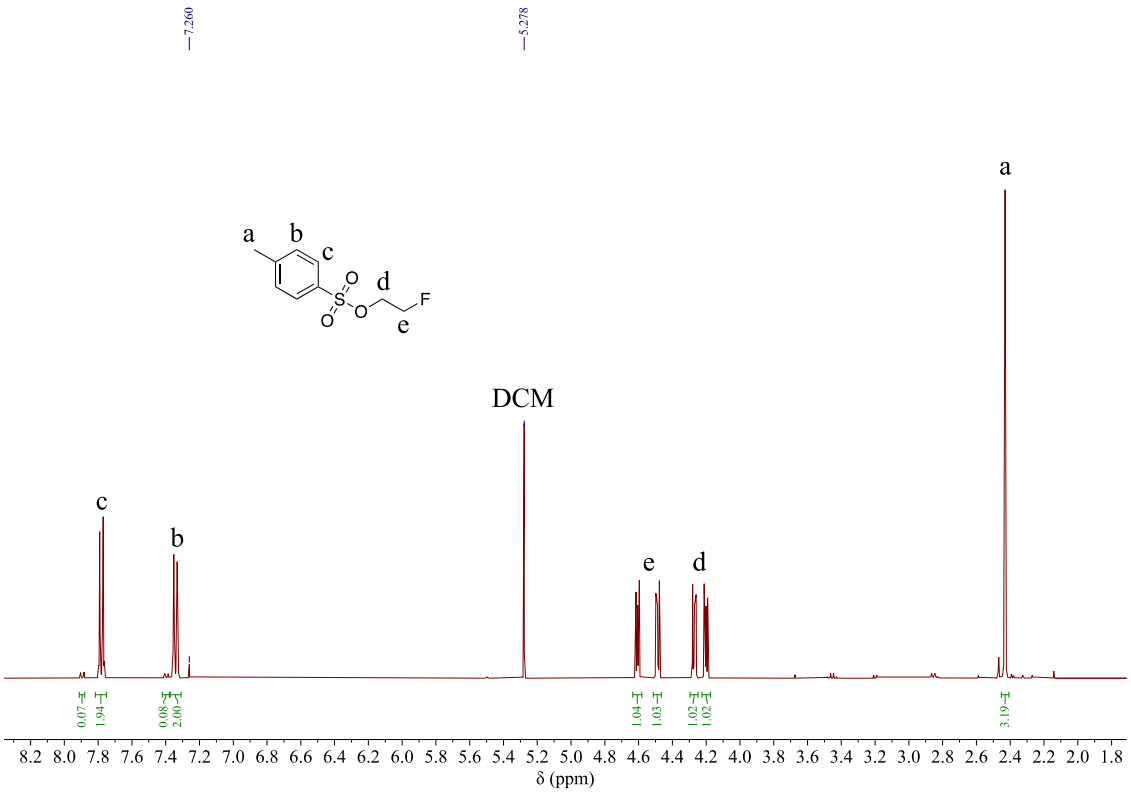

Figure S15 ^{1}H NMR spectrum ($CDCl_3$, 400MHz) of 2-fluoroehtyl tosylate. Crude contains ~4% tosyl chloride.

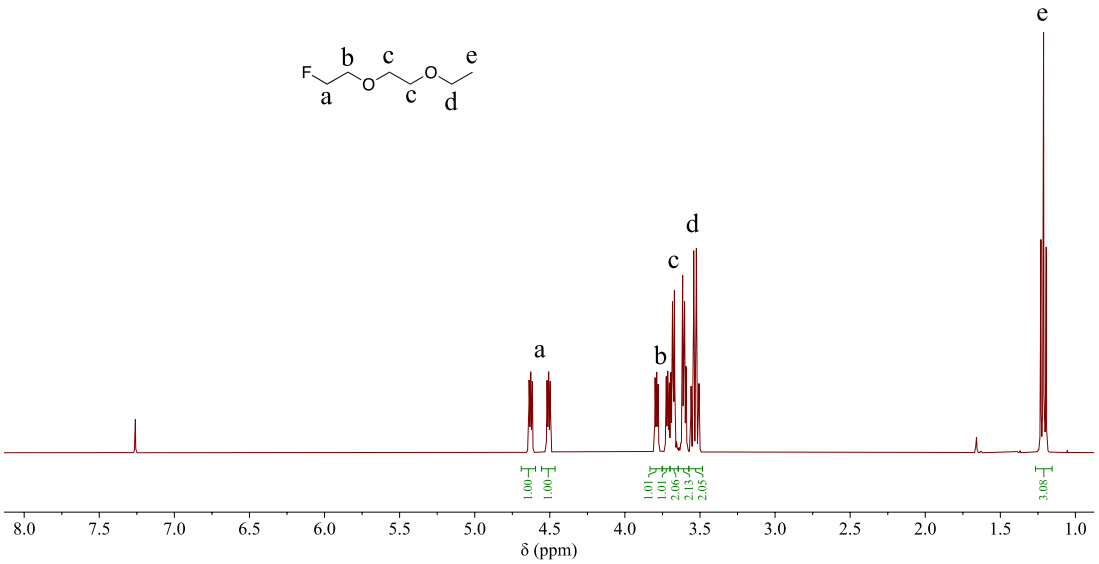

Figure S16 ^{1}H NMR spectrum ($CDCl_3$, 400MHz) of **F1F0** solvent molecule

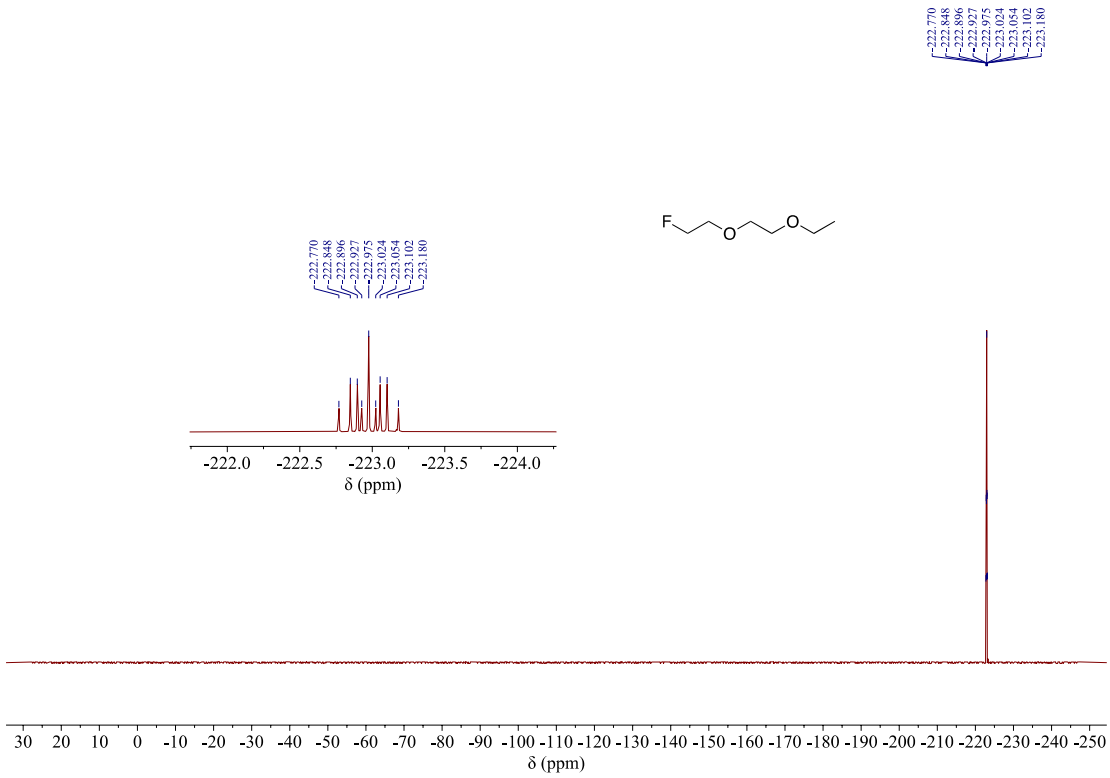

Figure S17 ^{19}F NMR spectrum ($CDCl_3$, 400MHz) of **F1F0** solvent molecule

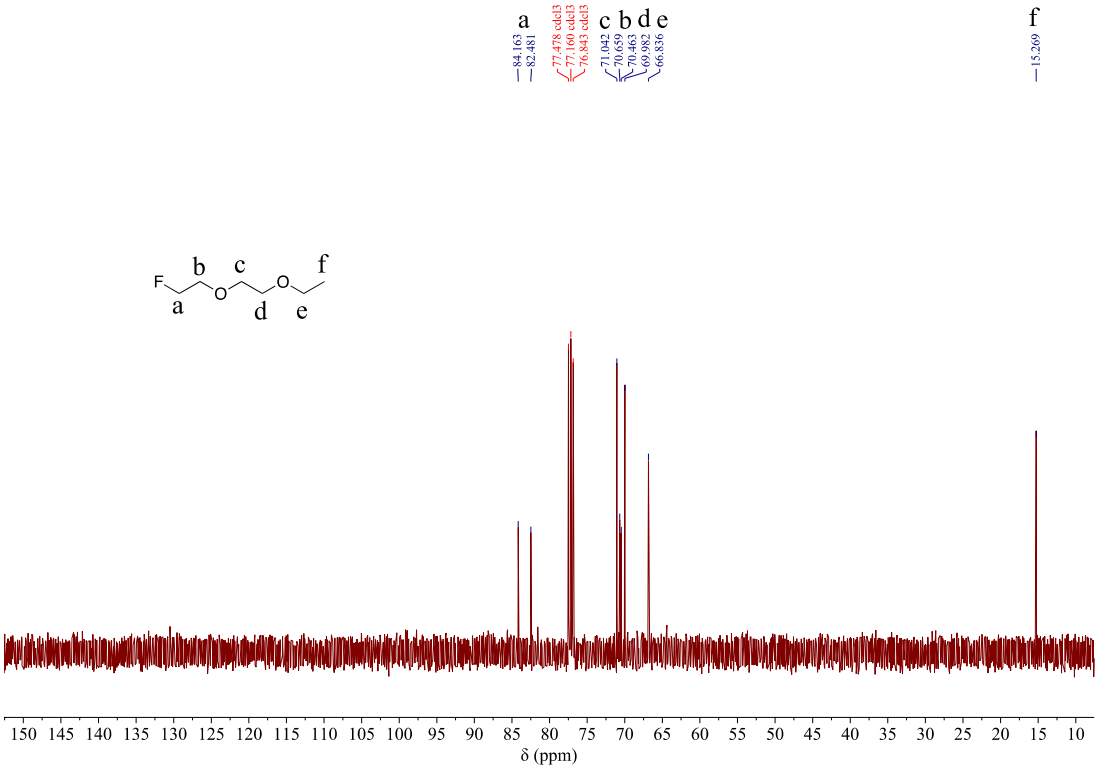

Figure S18 ^{13}C NMR spectrum ($CDCl_3$, 100MHz) of **F1F0** solvent molecule

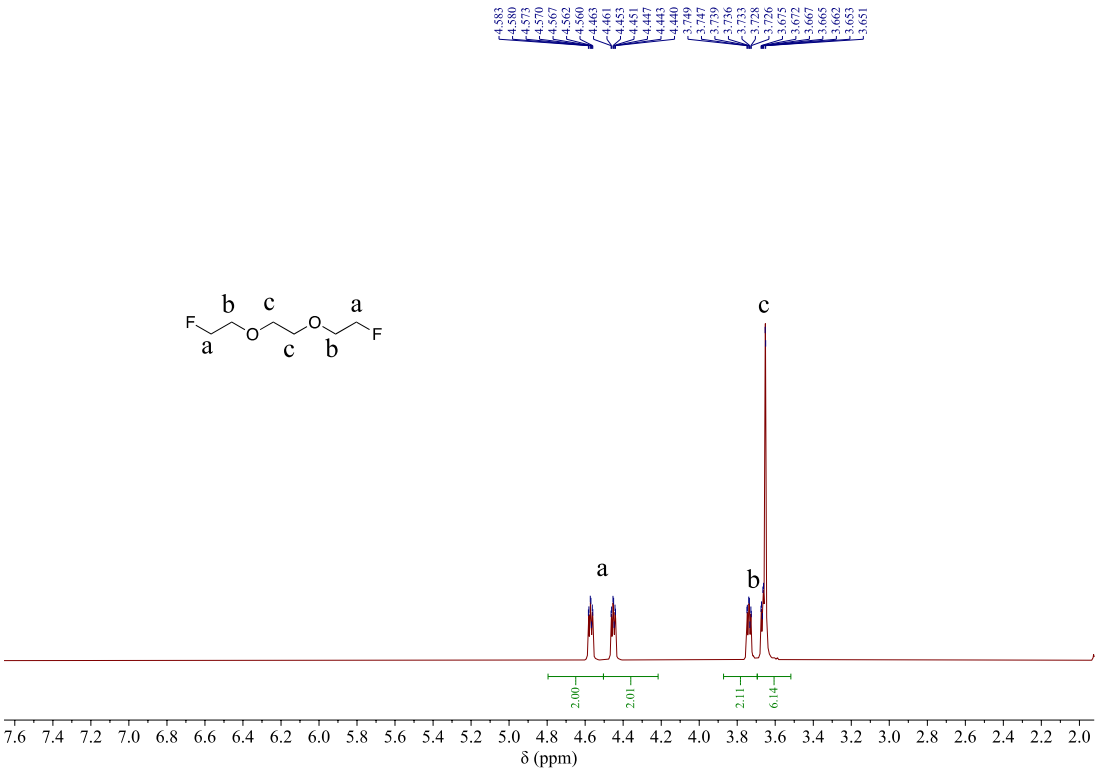

Figure S19 ^{1}H NMR spectrum ($CDCl_3$, 400MHz) of **F1F1** solvent molecule

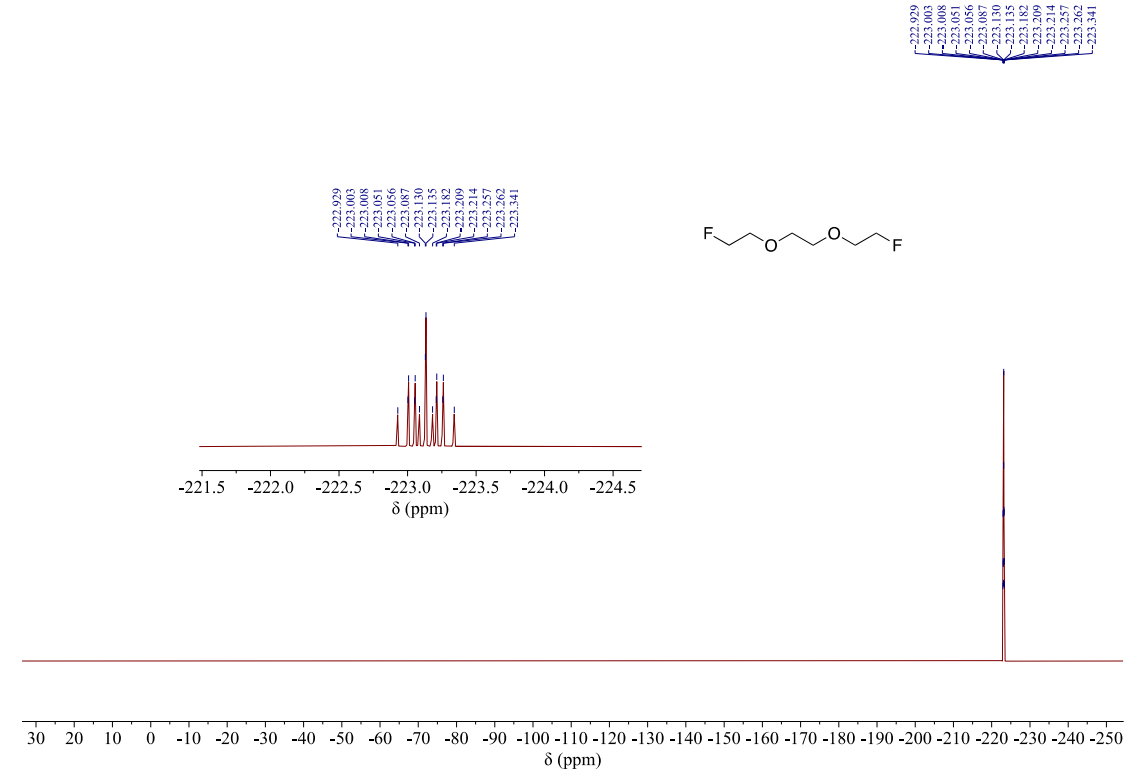

Figure S20 ^{19}F NMR spectrum ($CDCl_3$, 400MHz) of **F1F1** solvent molecule

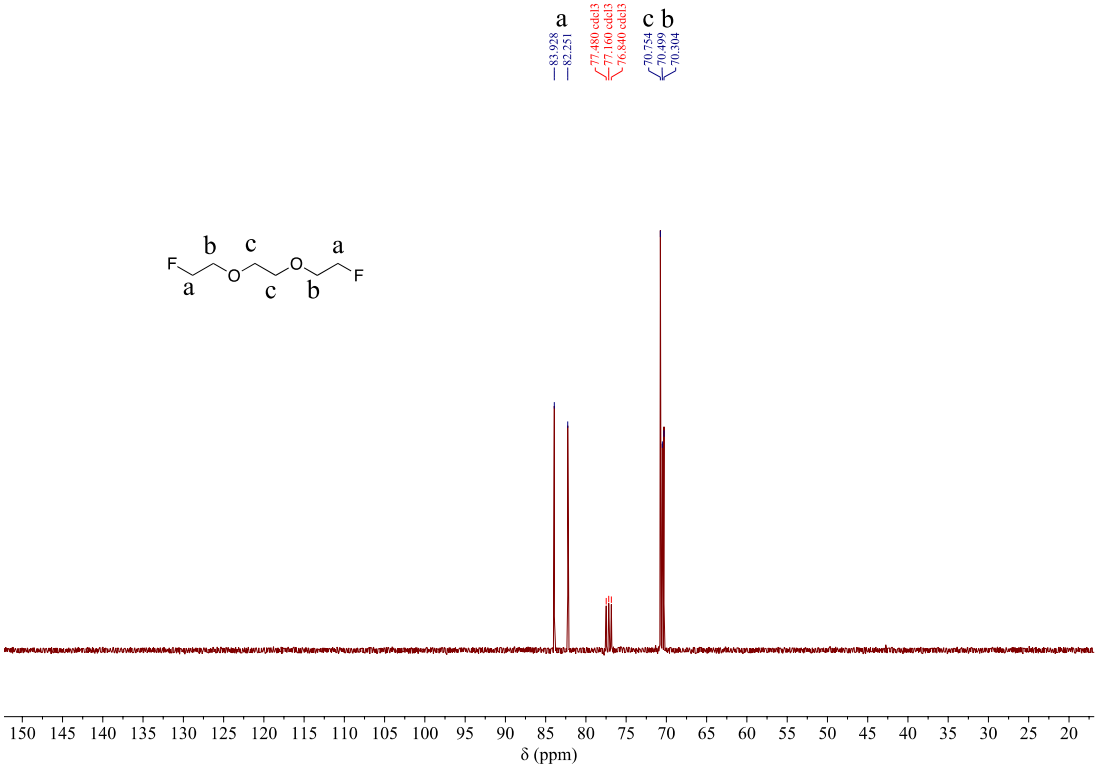

Figure S21 ^{13}C NMR spectrum ($CDCl_3$, 100MHz) of **F1F1** solvent molecule

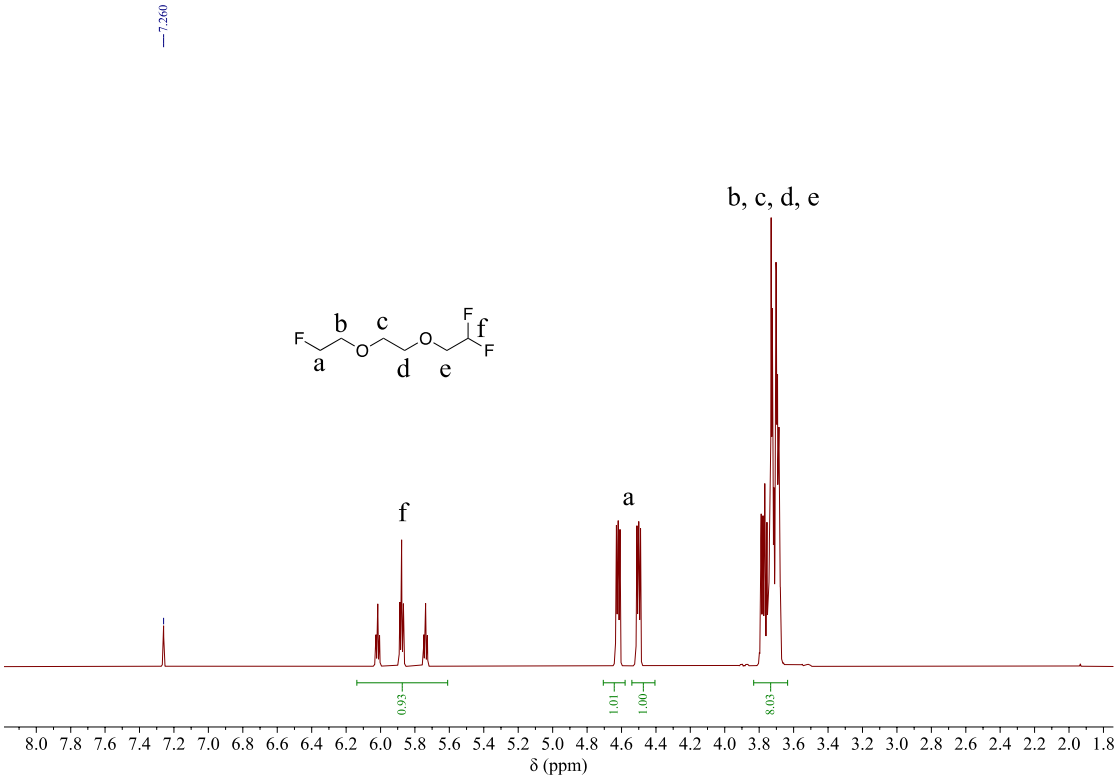

Figure S22 ^{1}H NMR spectrum ($CDCl_3$, 400MHz) of **F1F2** solvent molecule

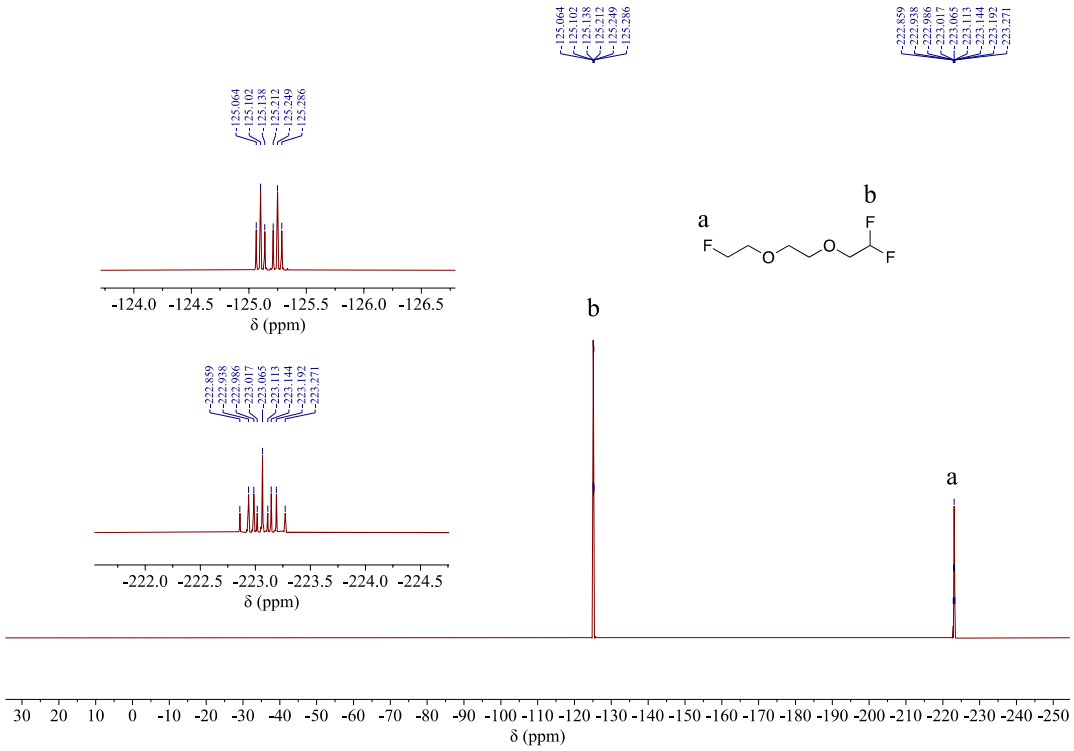

Figure S23 ^{19}F NMR spectrum ($CDCl_3$, 400MHz) of **F1F2** solvent molecule

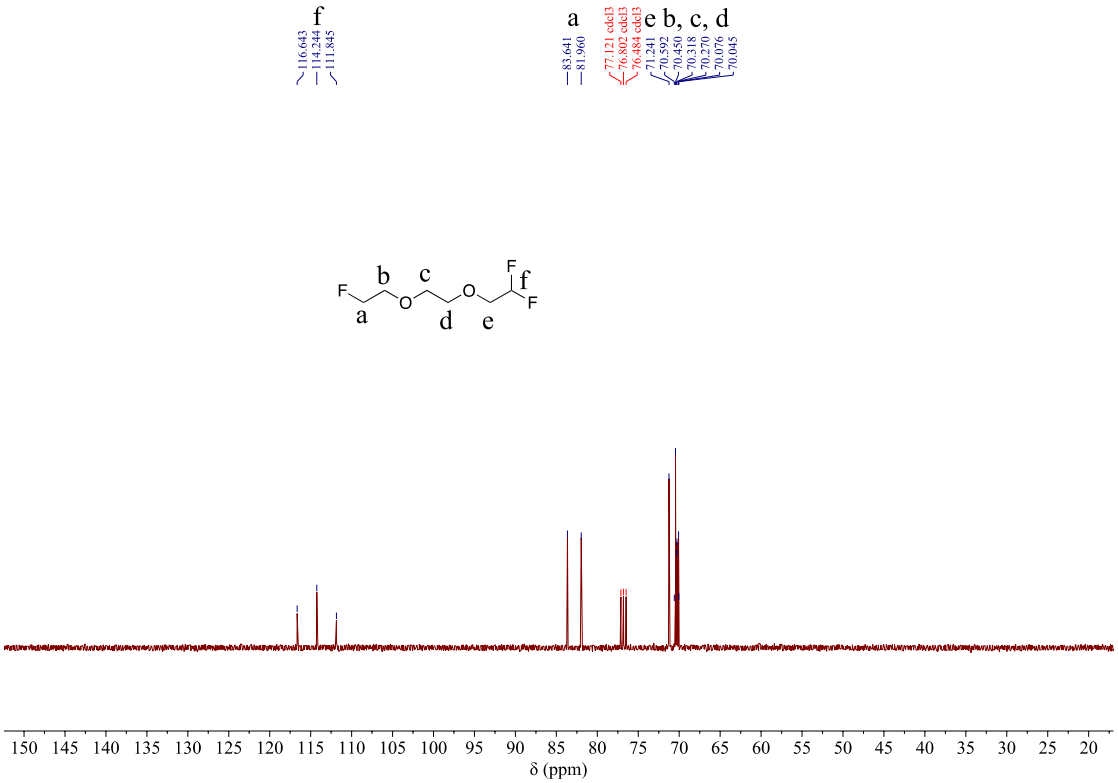

Figure S24 ^{13}C NMR spectrum ($CDCl_3$, 100MHz) of **F1F2** solvent molecule

XII. Reference

(1) Abraham, M. J.; Murtola, T.; Schulz, R.; Páll, S.; Smith, J. C.; Hess, B.; Lindahl, E. GROMACS: High performance molecular simulations through multi-level parallelism from laptops to supercomputers. *SoftwareX* **2015**, *1*, 19-25. DOI: 10.1016/j.softx.2015.06.001 (acccessed 2023/05/19).
(2) Wang, J.; Wolf, R. M.; Caldwell, J. W.; Kollman, P. A.; Case, D. A. Development and testing of a general amber force field. *Journal of Computational Chemistry* **2004**, *25* (9), 1157-1174, https://doi.org/10.1002/jcc.20035. DOI: https://doi.org/10.1002/jcc.20035 (acccessed 2023/05/19).
(3) Sousa da Silva, A. W.; Vranken, W. F. ACPYPE - AnteChamber PYthon Parser interfacE. *BMC Research Notes* **2012**, *5* (1), 367. DOI: 10.1186/1756-0500-5-367.
(4) Humphrey, W.; Dalke, A.; Schulten, K. VMD: Visual molecular dynamics. *Journal of Molecular Graphics* **1996**, *14* (1), 33-38. DOI: https://doi.org/10.1016/0263-7855(96)00018-5.
(5) Michaud-Agrawal, N.; Denning, E. J.; Woolf, T. B.; Beckstein, O. MDAnalysis: A toolkit for the analysis of molecular dynamics simulations. *Journal of Computational Chemistry* **2011**, *32* (10), 2319-2327, https://doi.org/10.1002/jcc.21787. DOI: https://doi.org/10.1002/jcc.21787 (acccessed 2023/05/19).
(6) Gowers , R. J.; Linke , M.; Barnoud , J.; Reddy , T. J. E.; Melo , M. N.; Seyler , S. L.; Doman´ski, J.; Dotson , D. L.; Buchoux , S. b.; Kenney , I. M.; et al. MD Analysis: A Python Package for the Rapid Analysis of Molecular Dynamics Simulations. In *PROC. OF THE 15th PYTHON IN SCIENCE CONF.*, Austin, Texas, 2016; Rostrup, S. B. a. S., Ed.; pp 98 - 105. DOI: 10.25080/Majora-629e541a-00e.
(7) Yu, Z.; Rudnicki, P. E.; Zhang, Z.; Huang, Z.; Celik, H.; Oyakhire, S. T.; Chen, Y.; Kong, X.; Kim, S. C.; Xiao, X.; et al. Rational solvent molecule tuning for high-performance lithium metal battery electrolytes. *Nature Energy* **2022**, *7* (1), 94-106. DOI: 10.1038/s41560-021-00962-y.